Directional solidification of dilute Sn–Pb alloys

H. Ochoa[1], O. Fornaro*[2], O. Bustos[3] and B. Schulz[3]

Microstructure evolution and pattern formation during directional solidification of dilute Sn–Pb system were analysed. Planar, cellular and dendritic morphologies were obtained by adequate thermal gradient and interface velocity control. The samples were obtained from pure elements in concentrations of 0·05, 1·0 and 4·0 wt-%Pb. Growth was carried out in a Bridgman device in the velocity range of 0·38–30 μm s^{-1} at thermal gradients from 1·3 to 2·6°C mm^{-1}. The samples were examined using metallographic techniques to determine their morphology and dimensional characteristics. The system was analysed to describe the different stages of evolution of the morphology and transitions. It was observed that both primary cellular and dendritic spacing decreased with increasing velocity. However, in the cellular–dendritic transition zone, an important increase in spacing was detected and basically associated with convective effects during irregular cellular growth.

Keywords: Non-ferrous alloys, Microstructure, Microsegregation, Directional solidification

Introduction

The thermal, chemical, electrical and mechanical properties of samples obtained by melting are influenced by segregation, grain size, porosity and cellular or dendritic spacing. These characteristics result from the thermosolutal behaviour and from metal–mould interaction during solidification, which is governed by the thermal gradient, the advance interface velocity and the chemical alloy composition. The importance of directional solidification in the control of microstructure was widely referenced in the literature.[1–4]

The morphological stability theory[5–7] defines the conditions under which a planar, solid/liquid interface (S-L) becomes unstable. According to this theory, at low and moderate solidification rates, the modified constitutional supercooling criterion can be applied

$$\frac{G^*}{VC_0} = \frac{m_L}{D_L}\,\frac{(k_0-1)}{k_0} \tag{1}$$

where G^* is the weighted average thermal gradient, corresponding to

$$G^* = (\kappa_L G_L + \kappa_S G_S)/\bar{\kappa} \tag{2}$$

where m_L is the slope of the liquidus line in the equilibrium phase diagram, D_L is the solute diffusion constant coefficient in the liquid state and k_0 is the equilibrium partition coefficient. κ_S, κ_L and $\bar{\kappa}$ are solid, liquid and average thermal conductivities. When the κ_S and κ_L phases are similar, the expression of Tiller *et al.*[8] can be considered valid by replacing G_L (thermal gradient in front of the interface) with G^*. From a qualitative point of view, the decrease in parameter (G_L/VC_0) controls the evolution of the structure from planar to dendritic morphologies. Different morphological stages have been experimentally obtained with decreasing (G_L/VC_0) for directional solidification of dilute metallic alloys with fcc structures:[3]

(i) S-L plane interface (constitutional stability)
(ii) nodes or depressions in the S-L interface
(iii) elongated or bidimensional cells
(iv) regular or hexagonal cells (non-linear stability)
(v) irregular cells
(vi) dendritic cells in cooperative growth.

The stability and existence of different stages are still under discussion, but several proposals exist for stages (i)–(iv) as well as for some of the transitions between them, i.e. (i)–(ii) (constitutional stability), (ii)–(iii) (non-linear stability), (i)–(iii)–(i) (criticality of transition), (v)–(vi) (cellular to dendritic growth) and (vi)–(vii) (absolute stability).[3] The cellular to dendritic transition was deeply studied both for transparent thin organic systems and for bulk metallic systems. The proposal of Kurz and Fisher[2,9] considers that there is a slope change in the plot of primary spacing against velocity during the cellular to dendritic transition. This happens for a value of G^*, V_{TR} and C_0 given by

$$\frac{G^*}{V_{TR}C_0} = \frac{m_L}{D_L}(k_0-1) \tag{3a}$$

or

[1]Departamento de Ingeniería Mecánica, Universidad de Antofagasta, Av. Angamos 601, Antofagasta, Chile
[2]IFIMAT: Instituto de Física de Materiales Tandil (FCE-CICPBA-MT), Universidad Nacional del Centro de la Provincia de Buenos Aires, Pinto 399 (B7000GHG) Tandil, Argentina and CONICET: Consejo Nacional de Investigaciones Científicas y Técnicas (CONICET)
[3]Departamento de Ingeniería Metalúrgica, Universidad de Santiago de Chile, Av. Bernardo O'Higgins No. 3363, Santiago, Chile

*Corresponding author, email ofornaro@exa.unicen.edu.ar

Received 26 October 2007; accepted 2 February 2012
DOI 10.1179/1743133612Y.0000000010

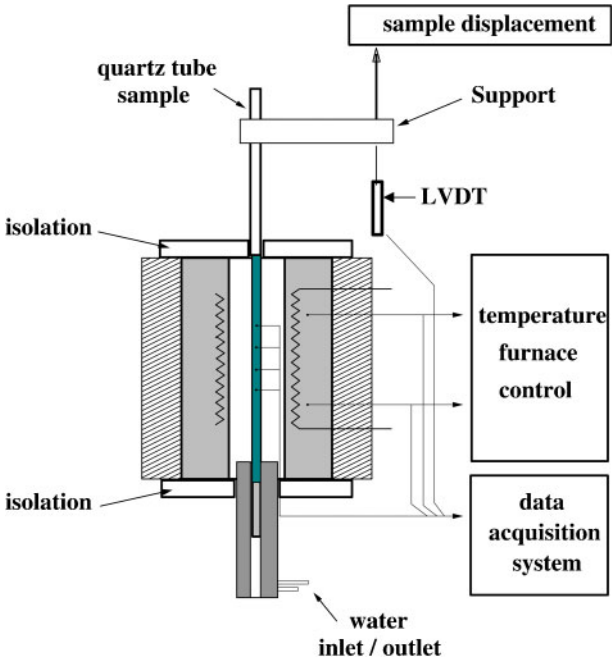

1 Schematic view of experimental device used in this work

$$V_{TR} = \frac{V_{CS}}{k_0} \tag{3b}$$

where V_{CS} corresponds to critical velocity for planar to cellular transition derived from equation (1).

During the experimental growth of tetragonal Sn base crystals, the evolution of morphology and the transition mechanisms may be different with respect to other systems. At present, only a few experimental studies exist to study the morphology evolution of dilute base Sn systems.[10–12] These works show that from planar to cellular, the morphologies are similar to that found in fcc alloys.[10] At higher growth rates, Biloni *et al.*[11,12] do not show evidence of cooperative dendritic growth for very dilute Sn–Pb alloys. Instead, only packets of cells inside a striation border or subgrains were detected. This structure is often called macromosaics in the literature. In addition to that, ordered dendrites were detected by Rocha *et al.* using a higher concentration of Sn–4 wt% Pb.

The aim of the present work is to study experimentally the formation of different microstructures during the directional solidification of tetragonal Sn–Pb alloys using detailed metallographic analysis of the obtained samples. Contributions can be made to the knowledge about the pattern development of microsegregation in samples directionally grown under different operational conditions and to the possible mechanisms associated with the transitions among the substructure stages mentioned above.

Experimental

Controlled directional solidification was obtained in a Bridgman-like device, as can be seen in Fig. 1. The device consists of two chambers located in a cylindrical symmetry. The upper chamber consists of an alumina core with a heating coil with electronic temperature control. The lower section is refrigerated by water circulation. Water flux is controlled by a valve.[14–17] This arrangement provides a thermal gradient at the point where the samples are located. The pulling system was based in a stepper motor and a gear box, which permitted translation velocity in the range of 0–10 μm s^{-1}. The displacement velocity was measured and controlled with a linear variable differential transformer and a signal conditioning interface, and the data were sent to a personal computer that drives the motor. This scheme provides very precise motion, resulting in a precision of $\pm 0{\cdot}1$ μm s^{-1}.[15,18]

The temperatures in the sample were taken using a double K type (CrNi–AlNi) thermocouple, which permits the determination of temperature and thermal gradient simultaneously. Measuring was by an Acquisition Data logger system, with an experimental error of $\pm 0{\cdot}5$ K. In this work, the thermal gradient was fixed in each set of experiments, taking the velocity as the control parameter of the problem.

Alloys of Sn containing 0·05, 1·0, 4·0 and 38·0 wt-%Pb were obtained by melting the pure elements in an electrical furnace under a controlled Ar atmosphere. The ingots were located in a cylindrical quartz tube, where directional solidification was achieved. The experiments started by initially melting the samples at 320°C. Solidification was initiated using a source of low temperature in the lower part of the oven until a stationary state was reached. Relative movement between the sample and the furnace was then initiated.

The samples were quenched by an axial flux of water and then longitudinal and transversally cut using a diamond disc. The metallographic preparation of the surface consisted of mechanical polishing with SiC paper up to 600 grit and then with an alumina suspension (Stuers, 0·5 μm, grade 2) in a soft cloth. Electrolytic polishing was subsequently carried out using a solution of distilled water (13 mL), acetic acid (300 mL) and perchloric acid (63 mL), at 20–30 V, for periods of 20 s. Chemical etching with 35% acetic acid, 50% glycerine and 15% nitric acid solution gave adequate relief for optical microscopy.

Microscopic observation of the morphology was carried out in an optical metallographic microscope at different magnifications. Observation and measurement of the interface geometry were made by direct photographic measurement on the surface of the sample. Wavelength measurement of the primary spacing was measured between successive cellular or dendrite tips using an image acquisition system and the UTHSCSA Image Tool v3·0 Final (Dental Diagnostic Science, University of Texas Health Science Center at San Antonio).

Results and discussion

It is known that the non-faceted crystals that grow from the melt could assume a variety of morphologies, depending on the solidification conditions. These morphologies can be observed through quenching the growth and adequate metallographic techniques. In the micrographs of Figs. 2–4, it can be noted in qualitative terms that as the (G_L/VC_0) parameter decreases as a result of velocity or concentration increasing, or a decrease in the thermal gradient, the structure shows more complex morphologies from planar, to cellular and dendritic solidification fronts.

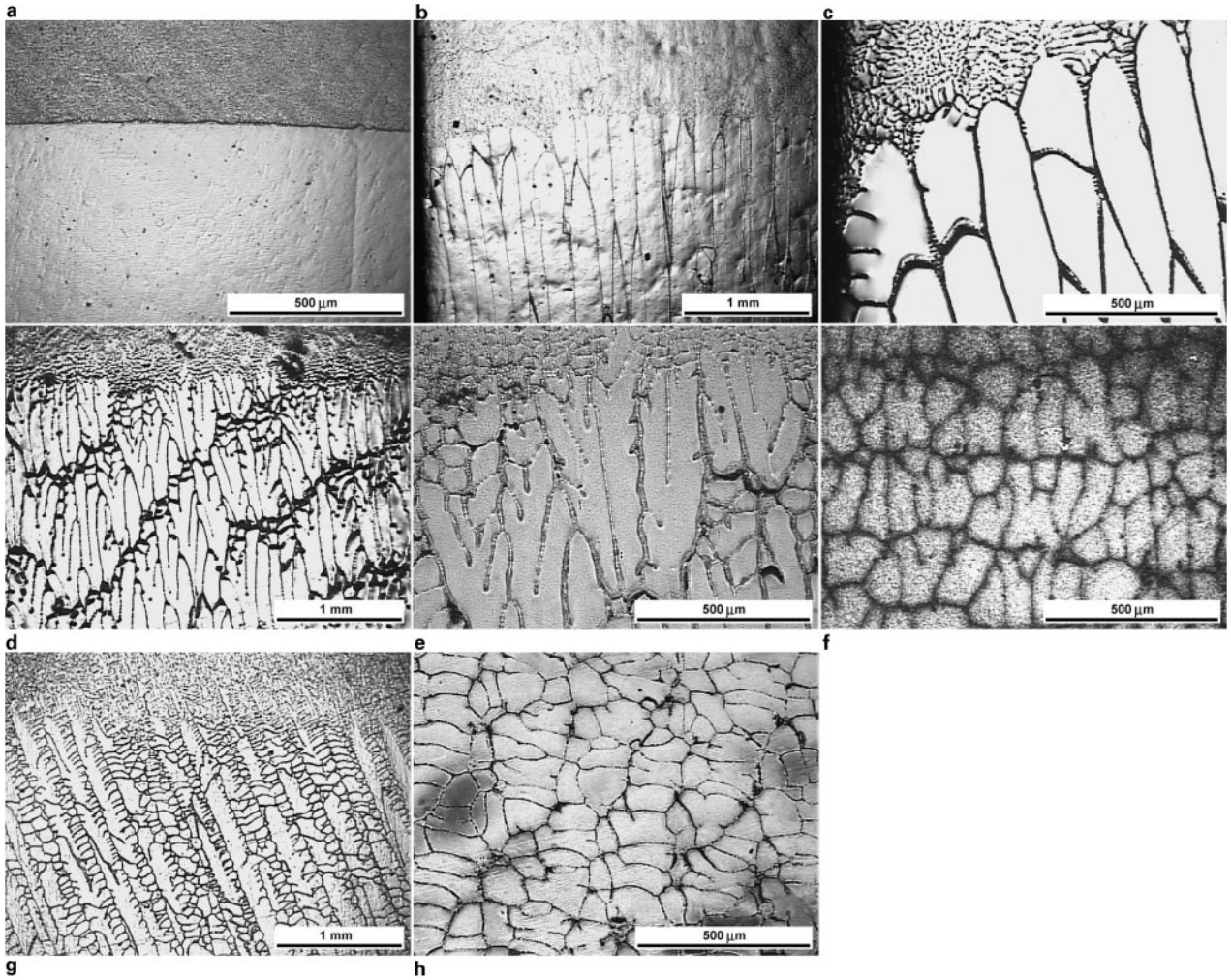

a planar interface, V=0·426 μm s^{-1}, G_L=1·88 K mm^{-1}; *b* regular cells, V=2·53 μm s^{-1}, G_L=2·02 K mm^{-1}; *c* irregular cells, beginning transition, V=4·15 μm s^{-1}, G_L=2·12 K mm^{-1}; *d–f* macromosaic microstructure, V=13·02 μm s^{-1}, G_L=1·9 K mm^{-1}; *e* longitudinal section; *f* transverse section, at 450 μm behind S-L interface; *g*, *h* dendritic morphology, V=22·2 μm s^{-1}, G_L=2·2 K mm^{-1}; *g* longitudinal section; *h* transverse section at 250 μm behind S-L interface

2 Microstructure of Sn–1 wt% Pb directionally grown

Figure 2 shows the morphological evolution for C_0=1·0 wt-%Pb. The sequence was obtained for different growth velocities, while the thermal gradient was maintained in the order of 2°C mm^{-1}. The microstructure shows planar interfaces under velocities of 0·426 μm s^{-1}, as can be seen in Fig. 2*a*. It can also be noted that at the grain boundary, an additional perturbation appears. This perturbation does not have an influence in the solid but appears to be propagated in the quenched zone. Regular type cells can be noted in Fig. 2*b*. This structure has a regular spacing of λ_1=160 μm. Figure 2*c* shows the beginning of the transition from cells to irregular cells, reflected in the appearance of a larger quantity of arms and missing cellular walls, first at the periphery of the sample and later at the centre. Figure 2*e* and *f* shows an irregular microstructure for V=7·95 μm s^{-1} and G_L=1·92°C mm^{-1}. During this stage, macromosaic or packed cell morphology begins to appear during the transition from cellular to dendritic for this composition. This particular structure appears to be formed by multiple cells that are growing together, rounded by a higher segregated boundary, as can be seen in the transversal view of Fig. 2*f*. In the longitudinal view of the samples, we could observe that in certain opportunities, a pair of cells can grow joined, forming doublets or multiplets, as can be seen in Fig. 2*e*. A similar behaviour was reported during the directional solidification of thin samples[3,19–21] and could be explained as an effect of thermosolutal convection. Cooperative dendrites are shown in Fig. 2*g* and *h*. Characteristic secondary arms can be seen in these figures, in a similar way to fcc crystal growth. In Fig. 2*g*, the dendrites are aligned in the preferential growth direction, which is not parallel to the heat extraction. In Fig. 2*h*, a transversal dendritic microstructure can also be seen.

Figure 3 shows a similar evolution for the Sn–4Pb (wt-%) alloy. From Fig. 3*a–d*, the velocity is increasing, fixing the thermal gradient in the order of G_L= 2·5°C mm^{-1}. Shallow and deep cells can be seen in Fig. 3*a* and *b* respectively. The structure appears irregular, with segregated channels of different widths. At greater velocities, the structure becomes, in general, more disordered, showing thin cells that are growing together. Figure 3*c* shows this kind of structure with greater detail. In Fig. 3*d*, it is possible to see dendritic growth at a velocity of V=11·5 μm s^{-1}.

In accord with our experiences, the cellular to dendritic transition appears to be a competition between macromosaic and dendritic structures, in that both can co-exist at the same time in bulk samples in a given

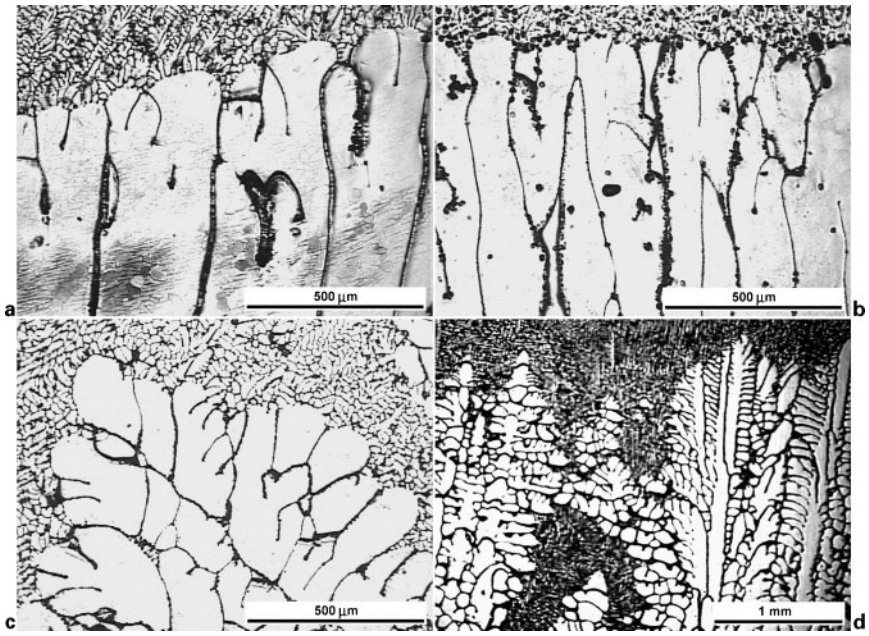

a V=2·0 μm s^{-1}, G_L=2·5 K mm^{-1}; *b* V=3·1 μm s^{-1}, G_L=2·5 K mm^{-1}, cellular growth; *c* V=7·5 μm s^{-1}, G_L=2·5 K mm^{-1}, several irregular cells forming dendrite; *d* V=11·5 μm s^{-1}, G_L=2·45 K mm^{-1}, dendritic growth

3 Microstructure of Sn–4 wt% Pb directionally grown

range of interface velocities. This range seems to be dependent on composition, being thinner at greater concentrations. For example, at C_0=4 wt-%Pb, it can be noted that the macromosaic structure appears less frequently, dendritic growth being the preferred morphology. In samples grown at C_0=1 wt-%Pb, irregular cells and macromosaics clearly appear before cooperative dendritic morphology. The results of the present study show that these structures are highly unstable[21] and appear as a transition mechanism during cellular to dendritic transition, favoured by the effect of high thermosolutal convection.

Shallow cells were also detected with dilute 0·05 wt-%Pb alloys and shown in longitudinal view in Fig. 4*a* and as transversal view in Fig. 4*b* and *c*. Figure 4*a* shows shallow cells with a depth of 310 μm and a spacing of 148 μm. A second order of periodicity is also observable on the interface, which is represented as three-cell packets, with an approximate wavelength of 413 μm. Figure 4*b* shows the transverse section of this cell, 170 μm behind the interface, where well defined packing can be observed. A better formed cell structure is shown in Fig. 4*c*. In addition, a large number of nodes are found in the corners and lateral

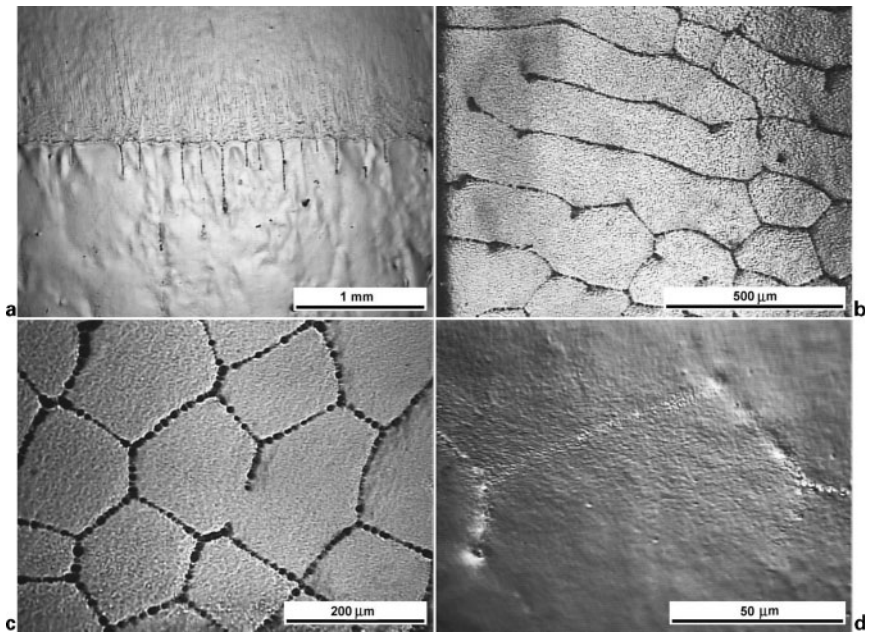

a–c shallow cells, V=7·5 μm s^{-1}, G_L=2·5 K mm^{-1}; *a* longitudinal section; *b* transverse section, at 170 μm behind S-L interface; *c* distribution of nodes on cellular walls; *d* V=24·87 μm s^{-1}, G_L=2·45 K mm^{-1}, transverse section of cell showing vertex and wall high concentration nodes

4 Microstructure of Sn–0·05 wt% Pb

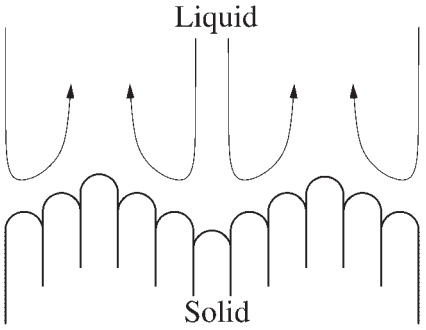

5 Schematic drawing showing presence of convection in longitudinal view of directional solidification sample

walls. Figure 4*d* shows a detail of the cellular walls at higher velocity.

Owing to the different densities of tin and lead, it is necessary to include thermosolutal convection in the interpretation of the microstructures. The thermosolutal convection affects the growth morphology and so the morphological transtions and macro- and microsegregation in the grown samples.[22,23] The profile of density in the liquid plays a fundamental role in the start of convection. This situation can be schematised in Fig. 5, where the presence of convection suggests that there exist zones with different compositions, making that richer zones could advance slower than the neighbour, affecting the macroscopic interface morphology. The effect of convection has the consequence of deforming periodically the interface, resulting in the clustering of cells and dendrites.

The behaviour is summarised in Fig. 6. Figure 6*a* (0·05%Pb) shows the planar and cellular zones. No dendritic growth was detected for this composition. A macromosaic microstructure appears only faintly through the second order spacing on the longitudinal view of the S-L interface. The behaviour at 1 and 4%Pb (Fig. 6*b* and *c* respectively) is similar, showing an increase in spacing during the cellular to dendritic transition. In this zone, a macromosaic structure was also detected. The experimental values found for planar to cellular transition were in good agreement with the constitutional supercooling criterion calculated using equation (1), while the cellular to dendritic transitions were in the order of Kurz and Fisher's proposal,[2,9] equation (3). Note, however, that this proposal does not take into account hydrodynamic instability nor convection effects. The present observations suggest that a range of co-existence of irregular cells growing in macromosaics and dendrites exists. These results are summarised in Table 1.

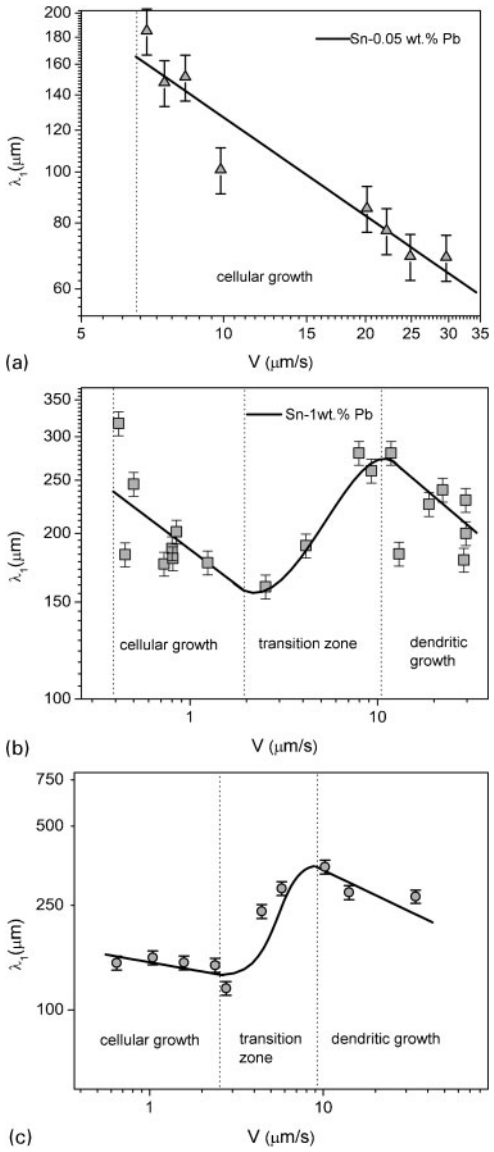

a **Sn–0.05 wt.% Pb;** ***b*** **Sn–1 wt.% Pb;** ***c*** **Sn–4 wt.% Pb**

6 Primary spacing against velocity of S-L interface

Conclusions

During directional solidification of bulk samples of dilute Sn–Pb alloys, it was possible to observe a variety of microstructures, planar interface, nodes, shallow cells, regular cells, irregular cells, packed cells and dendrites, depending on the solidification conditions and the concentration of the alloy. At low velocities, the change from planar to cellular growth was found similar to fcc systems, and critical velocities for transition were consistent with constitutional supercooling criteria. It

Table 1 Comparison of experimental and theoretical transition velocities

	Planar to cellular		Cellular to dendritic	
Pb/wt-%	Estimated/μm s^{-1}	Experimental/μm s^{-1}	Estimated/μm s^{-1}	Experimental/μm s^{-1}
0·05	6·22	6·88	95·40	…
1	0·311	0·426	4·77	4·15
4	0·078	0·0628	1·12	2·38

*G_L=2·5 K mm^{-1}.

is important to mention that in characterising the microstructure, it becomes necessary to include convection effects due to the different densities of solute and solvent. Lead being heavier than tin, convection effects are always present, which result in an hydrodynamic instability and a periodic composition profile ahead the interface that favour clustering and macromosaic formation under cellular and dendritic growth regimes. In this way, the cellular to dendritic transition was characterised by a competition between the formation of packed cells and dendrites. In very dilute regimes, cellular growth shows a high morphological stability and was not possible to obtain dendritic growths in the range of velocities studied.

Acknowledgements

The authors thank Professor H. Biloni for helpful discussions. The work was carried out at IFIMAT (CICPBA-MT, UNCPBA) and supported partially by SeCAT-UNCPBA, ANPCyT and CONICET. One of the authors (HO) thanks MECESUP, Universidad de Antofagasta and Universidad de Santiago de Chile for economical support. They would also like to express appreciation for the technical support given by O. Toscano at IFIMAT.

References

1. W. J. Boettinger, S. R. Coriell, A. L. Greer, A. Karma, W. Kurz, M. Rapaz and R. Trivedi: *Acta Mater.*, 2002, **48**, 43–70.
2. W. W. Kurz and D. J. Fisher: 'Fundamentals of solidification', 3rd edn; 1984, Aedermannsdorf, Trans. Tech Publications Ltd.
3. H. Biloni and W. J. Boettinger: 'Solidification', in 'Physical metalurgy', 4th edn, Ch. 8, 669–840; 1996, Amsterdam, Elsevier Science Publishers.
4. R. Trivedi, P. Mazumder and S. N. Tewari: *Metall. Mater. Trans. A*, 2002, **33A**, 3763–3774.
5. R. F. Sekerka: *Physica D*, 1984, **12D**, 212–214.
6. S. R. Coriell, G. B. McFadden and R. F. Sekerka: *J. Cryst. Growth*, 1990, **100**, 456–466.
7. S. R. Coriell and G. B. McFadden: 'Morphological stability', in 'Handbook of crystal growth', Ch. 12, 785–857; 1993, Amsterdam, North Holland.
8. W. A. Tiller, K. A. Jackson, J. W. Rutter and B. Chalmers: *Acta Metall.*, 1953, **1**, 428–437.
9. W. W. Kurz and D. J. Fisher: *Acta Metall.*, 1981, **11**, 11–20.
10. H. Biloni and G. F. Bolling: *Trans. TMS-AIME*, 1963, **227**, 1351–1360.
11. H. Biloni, G. F. Bolling and S. Cole: *Trans. TMS-AIME*, 1965, **233**, 251–252.
12. H. Biloni, R. Di Bella and G. F. Bolling: *Trans. TMS-AIME*, 1967, **239**, 2012–2013.
13. O. L. Rocha, C. A. Siqueira and A. Garcia: *Mater. Sci. Eng. A*, 2003, **A37**, 59.
14. O. Fornaro and H. A. Palacio: *Scr. Mater.*, 1997, **36**, 439–445.
15. O. Fornaro and H. A. Palacio: *Scr. Metall. Mater.*, 1994, **31**, 1265–1270.
16. O. Fornaro, H. A. Palacio and H. Biloni: *Mater. Res. Soc.*, 1998, **481**, 21–26.
17. O. Fornaro, H. A. Palacio and H. Biloni: 'Solidification processes and microstructures. A symposium in honor to Wilfried Kurz', 219–224; 2004, Warrendale PA, The Mineral, Metals, Materials Society.
18. O. Fornaro, H. Palacio and H. Billoni: *Mater. Sci. Eng. A*, 2006, **A417**, 134–142.
19. T. A. Brener, H. Muller-Krumbhaar and D. Temkin: *Phys. Rev. E*, 1996, **54E**, 2714–2722.
20. T. A. Brener and H. Muller-Krumbhaar: *Phys. Rev. E*, 1997, **55E**, 7780–7792.
21. S. Akamatsu, G. Faivre and I. Thomas: *Phys. Rev. E*, 1995, **51E**, 4751–4773.
22. S. N. Tewari, R. Shah and M. A. Chopra: *Metall. Mater. Trans. A*, 1993, **24A**, 1661–1669.
23. S. N. Tewari, Y.-H. Geng, G. L. Ding and R. Trivedi: *Metall. Mater. Trans. A*, 2002, **33A**, 1229–1243.